Reprinted from the Preprint Volume of the Third Intl. Conference on the Aviation Weather Systems, Jan. 30-Feb. 3, 1989, Anaheim, Calif. Published by the American Meteorological Society, Boston, Mass.

1.14

Weather Sensing with Airport Surveillance Radars

Mark E. Weber
MIT/Lincoln Laboratory
P.O. Box 73
Lexington, Massachusetts 02173-0073

I. Introduction

Modern airport surveillance radars (ASR) are coherent, pulsed-Doppler radars used for detection and tracking of aircraft in terminal area air space. The Federal Aviation Agency (FAA) is procuring over 100 next-generation ASR-9 radars for major U.S. airports while relocating existing ASR-8s to secondary terminals. Thus within the next five years, almost every U.S. airport that supports commercial operations will be equipped with one of these sensitive, highly stable S-band radars. In view of their on- or near-airport location, rapid scan rate and direct data link to air traffic control personnel, it has been recognized that ASRs can also provide flight controllers with timely information on weather conditions that are hazardous to aircraft.

An ASR's transmitted frequency, power, pulse-to-pulse stability and receiver sensitivity are well suited for weather sensing. Conversely, its broad elevation beamwidth, rapid antenna scan rate and non-uniform pulse transmission sequence introduce significant complications for the quantitative interpretation of echoes returned from weather. This paper reviews principal results of a four-year, FAA-sponsored program to evaluate the capabilities and limitations of ASRs for measuring storm severity.

The ASR-9 is equipped with a dedicated, digital signal processing channel to measure precipitation reflectivity and display any two of six calibrated levels (corresponding to the National Weather Service VIP levels) on the controllers' displays. In contrast to earlier FAA radars, precipitation echoes can be measured without the biases introduced by MTI circuits or circular polarization, and displayed without interfering with the radar's primary aircraft detection role. Section II describes this six-level reflectivity processor and summarizes our assessment of the quantitative accuracy of precipitation echoes as measured with the fast-scanning, fan beamed radar.

Section III treats a possible processor upgrade that would enable ASRs to measure the velocity of precipitation wind tracers and automatically detect regions of hazardous low altitude wind shear (LAWS). This capability is not a feature of current ASRs, but could be added without affecting the radars' other missions. The principal technical challenges for wind shear measurement and detection with an ASR involve ground clutter suppression, estimation of *low-altitude* radial velocity and achievement of operationally acceptable LAWS detection probabilities while maintaining false declarations at a low rate. Data from a field measurement program are presented showing that, at least for "wet" microburst induced wind shear, these challenges can be successfully met through appropriate data processing strategies.

The work described here was sponsored by the Federal Aviation Administration. The United States Government assumes no liability for its content or use thereof.

II. ASR-9 Six Level Reflectivity Processor

A. Processor Design

Figure 1 is a simplified block diagram of the ASR-9's six-level reflectivity processor. Digitized in-phase and quadrature signals are passed in parallel through an all-pass and three high-pass filters. As currently designed, the different filters attenuate scan-modulated ground clutter by an amount varying from 12 to 49 dB. Because of the high antenna scan rate and the resulting small number of pulses (8 or 10) available for clutter filtering, this attenuation requires that the filter -3 dB stop-bands extend 2 to 7 m/s to either side of zero. To minimize the resultant attenuation of weather echoes with low radial velocity, a "clear day map" containing *a priori* information on the distribution of ground clutter is used to select the appropriate filter output independently for each resolution cell. The selection criterion effectively considers both the intensity of clutter and the intensity of the weather in the resolution cell; the result is use of the least attenuating filter possible that still suppresses ground clutter sufficiently to eliminate false weather threshold crossings.

The resulting, filtered data streams are thresholded against the six NWS VIP levels using range-dependent thresholds that may include corrections for beamfilling loss (see B.3 below). These single resolution cell threshold crossings are smoothed over 1 nmi in range to produce the highest weather level present in eight or more of sixteen contiguous cells. Additional smoothing involves median filtering over successive antenna scans and over nearest neighbor cell clusters. A final spatial filtering stage causes weather contours to expand slightly so as to ensure that small regions of high reflectivity will be easily discernible on air traffic control displays.

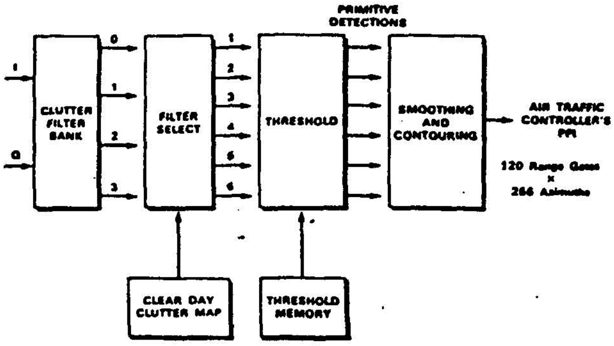

Figure 1. Block diagram of ASR-9 six-level weather processor.

Any two of the six available levels are selected by buttons on the control console; these are displayed using two levels of intensity modulation.

B. Assessment of Reflectivity Data Relative to Operational Needs

1. Statistical Stability of Displayed Weather Regions

One of the potential problems associated with the weather display is fluctuation of precipitation cell contours from scan to scan. This could give the impression that weather data are not being properly processed and are unreliable. In the ASR-9, single resolution cell weather level estimates are generated using only one pulse (at the clutter filter outputs). To overcome the inherent noisiness of such estimates, a sequence of spatial and temporal smoothing filters are employed.

In Figure 2, we have used a Monte-Carlo simulation [Weber,1986] to illustrate the statistical spread in reported weather levels at the various stages in the smoothing sequence. The plots show the limits within which 90 percent of reported weather levels would fall as a function of the true weather reflectivity factor. At the output of the final spatial filtering stage, the width of the transition interval between weather levels has been reduced to 1-2 dB. On the controller's display, the statistical displacement of contour boundaries from scan to scan is determined by this transition width and the horizontal gradient of precipitation reflectivity at the boundary. In most cases of operational concern, reflectivity gradients will be 2 dB/km or more so that contour boundary fluctuations will be smaller than the 1/2 nmi by 1.4 degree resolution cell size of the ASR-9 weather map. Simulations and maps recorded from the ASR-9 in Huntsville, Alabama confirm this conclusion that, after smoothing, statistical fluctuations of the weather reports are not significant.

2. Ground Clutter

Conventional MTI circuits for clutter suppression may cause significant attenuation of weather echoes when the weather's mean Doppler velocity and spectrum width are low. As described above, the ASR-9 "adaptively" selects the degree of clutter suppression required on a resolution cell-by-cell basis.

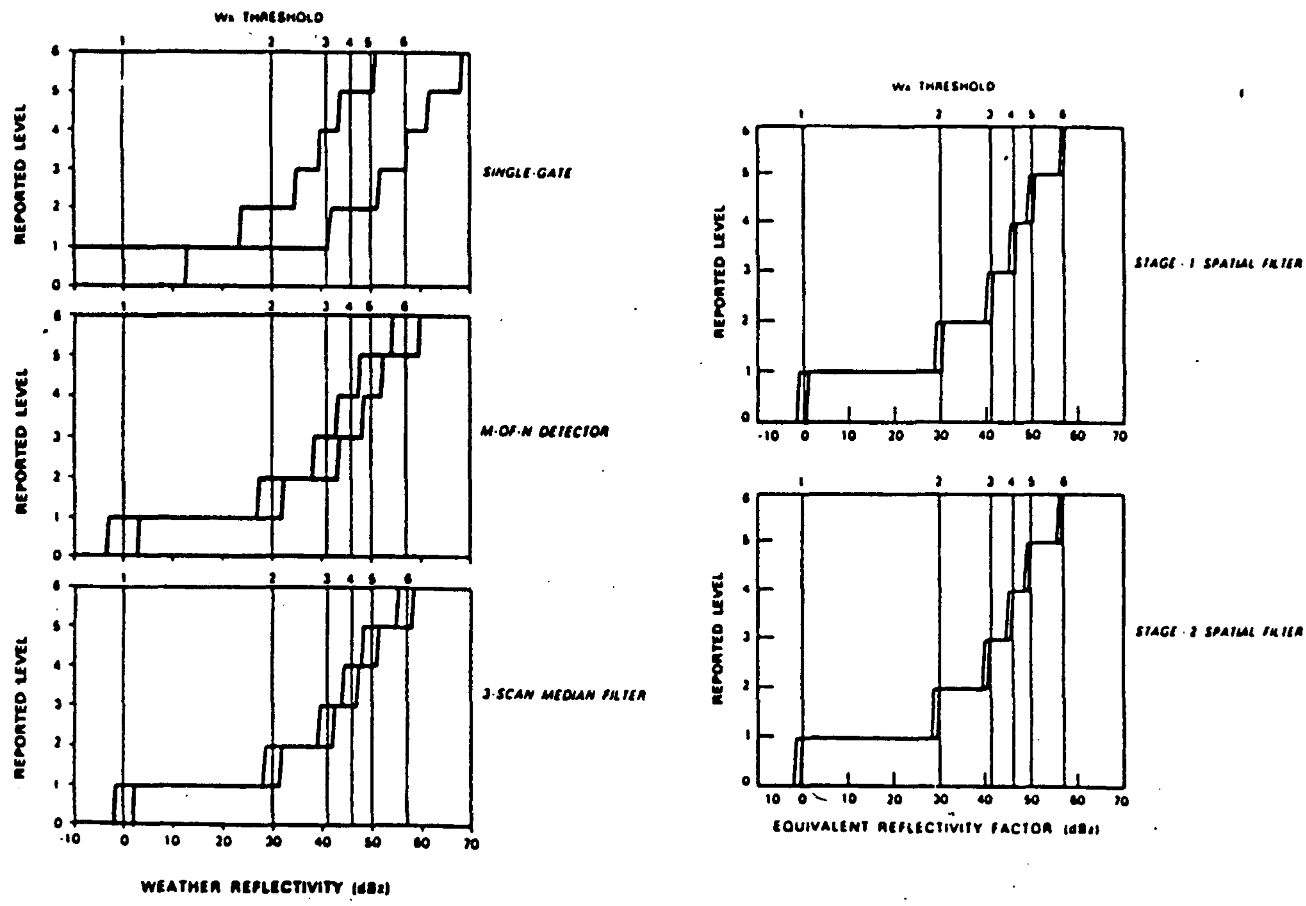

Figure 2. Statistical spread of ASR-9 weather reports. The two lines are the upper and lower limits within which 90% of the reports fall plotted as a function of weather reflectivity.

With this processing scheme, a probabilistic statement of the impact of ground clutter residue and the ground clutter filters on weather reflectivity estimates can be derived from the joint distribution of weather velocity, spectrum width and ground clutter intensity [Weber,1986]. Table 1 lists as a function of range and weather level, the probability for clutter-induced censoring or "significant" weather attenuation from the clutter filters using representative environmental measurements. The weather mean velocity and spectrum width distributions used in the calculation were derived from radar volume scans of thunderstorms and stratiform rain in the New England area; the ground clutter intensity distribution (which determines the proportion of resolution cells where clutter filtering must be invoked) was measured at Dallas-Ft. Worth Airport. "Significant" attenuation is defined relative to the size of the NWS levels which vary from 4 to 30 dB in extent.

Table 1: Probability for Censoring or Significant Attenuation of Weather Due to Ground Clutter

		Probability		
Wx Level	Significant Attenua-tion (dB)	0-5 nmi	5-10 nmi	10-15 nmi
1	27.	.43	.11	.09
2	8.3	.06	.03	.01
3	3.2	.07	.02	.02
4	2.5	.04	.02	.01
5	4.8	.01	.01	.00
6	5.6	.00	.00	.00

The table shows that -- with the exception of level one weather within 10 nmi of the radar -- ninety percent or more of the ASR-9's resolution cells should report the correct weather level in spite of the ground clutter. The spatial filters in the smoothing and contouring processor will, in general, further reduce the impact of ground clutter on the final weather maps. This robust clutter suppression capability has been confirmed with simulations and through field measurements with an ASR-8. We conclude that, in contrast to existing FAA and NWS radars, the ASR-9 weather channel should provide accurate precipitation reflectivity measurements even in the presence of intense ground clutter at short range.

3. Fan-Shaped Elevation Beam Pattern

The ASR-9 features dual cosecant-squared elevation receiving patterns with nominal 3 dB widths of 5 degrees. The "high" beam, employed at short range to reduce ground clutter intensity, has maximum gain about 6.5 degrees above the horizon. Beyond roughly 10 nmi, the receiver is switched to the "low" beam with peak response at 2 degrees elevation. At long range, the fan beam integrates precipitation echoes over much or all of a storm's depth; if the beam volume is only partially filled with precipitation, the measurement will underestimate even the vertically averaged reflectivity. At short range, the fixed elevation scan results in maximum sensitivity for precipitation in the lower portion of the storm.

The ASR-9 uses programmable, range-dependent weather thresholds which can be set so as to reduce reflectivity estimate biases caused by the beam pattern. As the processor is currently configured, these thresholds are quasi-static -- to be set up, for example, on a site-season dependent basis. Weber (1986) examined the performance of this technique using pencil-beam. Doppler radar volume scans from summertime storms in Eastern Massachusetts. Each volume scan was resampled onto a Cartesian coordinate grid. Fixing the x,y coordinates then defined a profile of precipitation reflectivity versus height. From the resulting ensemble of reflectivity profiles, range-dependent threshold corrections were derived that minimized the least squares difference between the (corrected) ASR-9 reflectivity estimate and a two-dimensional parameterization of the three-dimensional reflectivity field. In this section we treat one example of such a parameterization, the maximum reflectivity (over elevation angle) for each range-azimuth resolution cell.

Figure 3 plots an example of the average vertical distribution of reflectivity (relative to the peak) and the corresponding threshold correction; the figure was derived from that subset of the profiles where the maximum reflectivity corresponded to level three weather (41-46 dBz). The mean profile is flat up to 4 km (AGL) and falls off at an average rate of 3 dB/km at greater heights. Associated threshold corrections for the "maximum-in-height" reflectivity field parameterization approach 6 dB in the low beam at 60 nmi range. Results from subsets of the profiles corresponding to other NWS levels are similar, aside from a weak trend towards more rapid fall-off of reflectivity factor with height as the precipitation level increases.

The efficacy of the derived beam-shape corrections was then tested against the individual storm cases by comparing simulated ASR-9 weather maps against "maximum-in-height" truth generated from the same Doppler radar volume scans. The simulation procedure included all important effects of the ASR antenna pattern and weather processor. Results from a number of such comparisons are shown in Figure 4

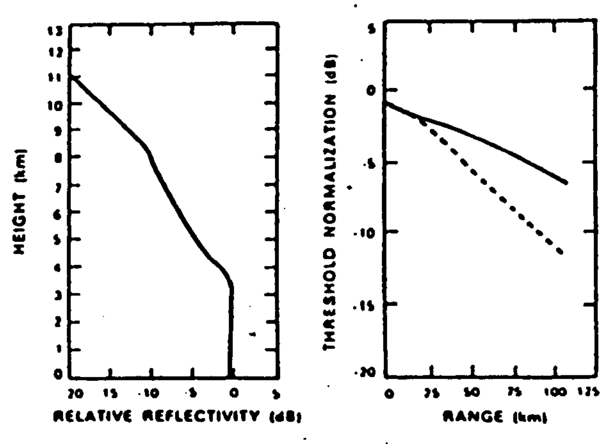

Figure 3. Mean profile of weather reflectivity versus height and corresponding weather threshold adjustment (Level 3 weather).

where the average error between simulated ASR reports and truth is plotted as a function of storm centroid range. This accuracy metric was calculated by means of a resolution cell-by-cell comparison and is approximately the fraction of resolution cells where the ASR report and truth differ.

Error probabilities are low, in the range 0.1 to 0.25. In most cases, the differences correspond to mismatch in size and shape of precipitation contours and not to actual missed detections or false alarms. The trend towards lower average error at long range was shown to indicate that the profile maximum reflectivity factor correlates more strongly with a vertically averaged (i.e. long range) ASR measurement than with its short range measurement of reflectivity in the lower part of the cloud.

Additional methods of accuracy assessment were discussed by Weber (1986) as was the accuracy of other possible two-dimensional parameterizations of the reflectivity field (e.g. averages over specified altitude intervals). Results were equivalent to those shown in Figure 4, indicating relative errors between ASR reports and "truth" that were generally no larger than 2 to 3 dB. This corresponds at most to a one level change in the reported NWS level.

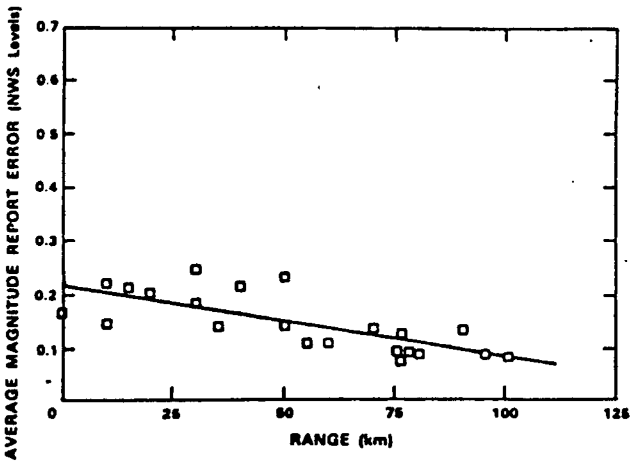

Figure 4. Average weather report error (NWS levels) versus storm range from radar.

III. Low Altitude Wind Shear Detection

During the last two decades, thunderstorm generated low-altitude wind shear has been identified as the primary cause of twelve major air-carrier accidents. In response to this hazard, the FAA has initiated a two-part enhancement to its terminal-area weather information network. The number of anemometers in the low-level wind shear alert system (LLWAS) is being increased and its detection algorithm reworked [Smythe,1988]. In addition, dedicated microwave terminal Doppler weather radars (TDWR) will be deployed at 50 to 100 airports to measure the radar reflectivity and radial velocity signatures associated with low altitude wind shear and to automatically report hazards to air traffic controllers [Turnbull *et al.*, 1988].

Augmentation of ASRs to provide a capability for LAWS detection could reinforce this deployment strategy in three areas. At airports not slated to receive TDWR or LLWAS, airport surveillance radars could work as stand-alone systems for providing controllers with LAWS warnings. The relatively low cost associated with equipping ASRs with wind-shear processors probably justifies this augmentation, even if the additional additional airports have low traffic volume or are in locales where wind shear is infrequent. At airports equipped with LLWAS but lacking a TDWR, reflectivity and wind measurements from an ASR could be used to reinforce LLWAS wind shear reports and to detect wind shear in operationally significant areas not covered by the surface weather stations. Even at airports with TDWR, additional radial wind measurements from a site well removed from the TDWR could reduce the possibility for error in estimated runway-oriented shear owing to microburst asymmetry [Weber and Noyes,1988]. In addition, the rapid scan rate of an ASR (12.5 per minute) would provide more frequent updates on wind shear than are currently planned for in the TDWR scanning schedule.

The following paragraphs summarize our analysis of the capabilities of ASRs for LAWS detection. More comprehensive discussion is provided by Weber *et al.*, (1987a,1987b,1988), Anderson (1987,1988) and Atlas (1988).

A. Experimental Facilities

Experimental results were obtained through analysis of data from two radar systems deployed near Huntsville, Alabama. A modified ASR-8, equipped with wide band recording capability was used for evaluating the capability of an airport surveillance radar to measure winds. In-phase and quadrature video signals from both receiving beams were recorded digitally on high density tape during periods of nearby thunderstorm activity. The radar could transmit either a constant pulse repetition frequency (PRF) or the 8/10 pulse alternating PRF waveform used by the ASR-9. Resulting data were transferred to computer compatible tape for off-line analysis.

The accuracy of radial wind fields measured by the airport surveillance radar was evaluated through comparison with volumetric reflectivity and radial velocity data from a colocated pencil beam Doppler weather radar. This radar operated at C-band, providing a 1.4 degree conical beam and range resolution of 250 m. The normal antenna scanning pattern combined low elevation angle PPI scans to determine the presence, aerial extent and intensity of thunderstorm outflows with RHI scans to measure the vertical structure of reflectivity and radial winds.

B. Principal Results

1. Sensitivity and Ground Clutter Suppression

Airport surveillance radars employ range dependent sensitivity control (STC) to prevent large targets such as ground clutter from saturating the receiver or A/D converters at short range. The limit for detection of low reflectivity thunderstorm outflows such as gust fronts or "dry" microbursts is therefore a function of the chosen STC setting as well as radar transmitter, antenna and receiver characteristics. Figure 5 plots the minimum detectable weather reflectivity factor (assuming 0 dB SNR requirement) versus range for an ASR-8 or ASR-9. The calculation assumed STC attenuation varying as the inverse square of range, with a cutoff at 23 km. Weber and Moser (1987) showed that, for representative ground clutter environments, this setting provided acceptable sensitivity while minimizing system saturation caused by the clutter. The curves also include "beamfilling" loss which accounts for that portion of the transmitted energy which does not intercept shallow, near-surface thunderstorm outflows. The different curves are for high (dashed) and low (solid) receiving beams, assuming outflow depths of 300 m or 500 m. Such values are representative of the depth of microburst outflows [Rinehart *et al.*, 1987].

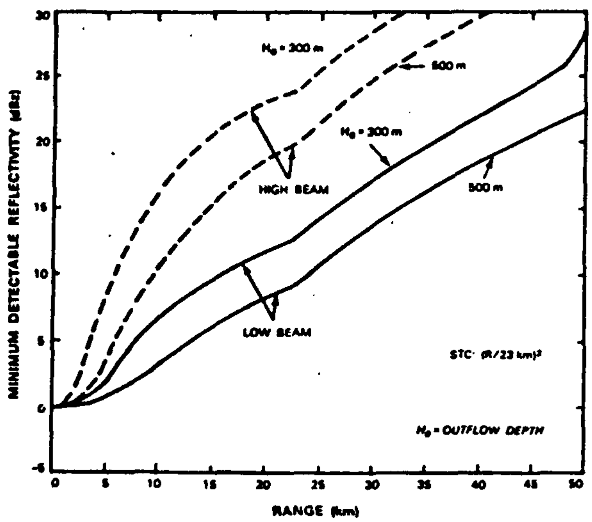

Figure 5. ASR-9 minimum detectable weather reflectivity factor including the beamfilling losses for 300 or 500 m deep thunderstorm outflows.

Given the on-airport location of ASRs, microburst detection is operationally relevant only over the range interval 0-12 km. Throughout this area, microburst outflows with reflectivity factor greater than about 10 dBz will be measurable with the low receiving beam. Using the same STC function, high beam sensitivity is about 10 dB poorer at 12 km range, owing to greater beamfilling loss. Gust front echoes frequently extend significantly higher than 500 m from the surface. Thus an ASR should be able to measure gust fronts with reflectivity factors greater than 10-15 dBz to at least 30 km range; this is sufficient to provide a useful forecasting capability for wind shifts at an airport.

Sensitivity considerations (above) and the need to maximize power received from near surface outflow layers relative to scatters aloft dictate that the low receiving beam of an ASR be used for wind shear detection, even at short range. This would result in intense interfering ground clutter. Weber (1987) used ground clutter measurements from our Huntsville ASR to analyze the performance of a specific clutter suppression scheme. A bank of FIR clutter filters was used to provide "adaptive" selection of the filter transfer function based on the intensity of clutter and of weather in each resolution cell. This procedure minimizes distortion of the weather echo spectrum in the filtering process. As proposed by Anderson (1987), the clutter filters would operate coherently across the PRF transitions of the ASR-9's waveform.

Figure 6 is illustrative of conclusions from our analysis. Here, simulated signals from a "microburst" have been combined with the measured ground clutter distribution to map out areas where the wind shear signature could be successfully extracted from clutter. The simulation took into account the stochastic nature of echoes from ground clutter as well as the prescribed signal processing approach. As a function of range, the fractional area *not* obscured by ground clutter is plotted assuming microburst reflectivity factors varying from 10 to 40 dBz. The plot shows that when the reflectivity factor exceeds about 20 dBz, fractional obscuration would be everywhere less than 0.3. In this situation, a microburst signature would normally be recognizable over at least part of its aerial extent. Conversely, recognition of very low reflectivity microbursts or gust fronts (10 Log Z << 20) at ranges less than 6 km may be difficult owing to ground clutter residue.

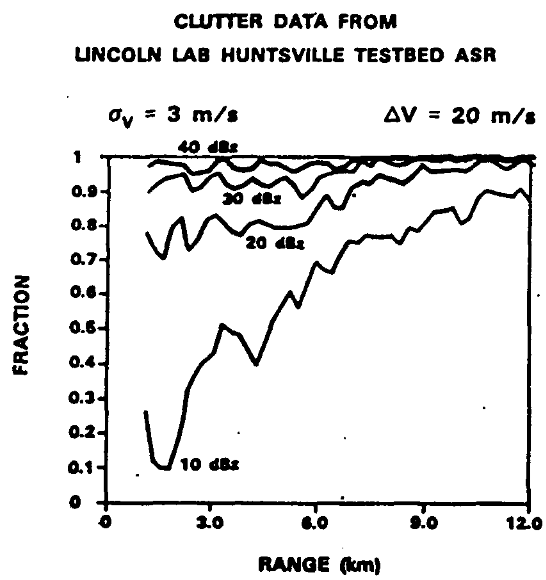

Figure 6. Fractional area not obscured by ground clutter as a function of range from the radar. Simulated microburst ΔV was 20 m/s, spectrum width was 3 m/s and reflectivity factor was as shown for the different curves.

2. Estimation of Low Altitude Radial Velocity

A significant problem for accurate low altitude velocity measurement with an ASR results from the bias introduced when energy is scattered into the elevation fan beam from precipitation aloft. This overhanging precipitation normally has a radial velocity markedly different from that in the outflow layer. As a result, a mean velocity estimate would be intermediate between the outflow velocity and radial winds aloft.

Figure 7 shows examples of velocity spectra measured with the testbed ASR in the radial velocity cores of Huntsville microbursts. Both high (dashed) and low (solid) beam spectra are displayed. The plots in the left column are for the approaching core and those in the right for the corresponding receding core. The spectra have been normalized to have the same integrated area. For reference, low elevation angle (0.7 degree) mean radial velocities measured at the same locations and times with the pencil beam radar are indicated by dashed vertical lines.

Relative to the pencil beam measurements, these spectra show significant RMS width (2-10 m/s) owing to the ASR's elevation beam pattern and the strong vertical shear in the wind field above microbursts. As a result, power weighted mean velocity estimates are significantly displaced from the pencil beam measurement; the result is an underestimate of wind shear as measured by the ASR which is greater for the high beam than the low beam, and which generally increases with range.

Signal processing techniques to overcome this problem attempt to separate spectral components scattered by low altitude thunderstorm outflows from those produced by winds aloft. Examples are:

(a) use of a high-pass filter to take advantage of the observation that microburst outflow winds are normally higher in absolute magnitude than winds aloft [Anderson.1988];

(b) comparison of amplitude spectra between high and low receiving beams [Weber and Noyes,1988; Atlas,1987,1988]. Low beam gain exceeds that in the high beam only at elevation angles below 5 degrees with the difference increasing monotonically as the horizon is approached. As seen from Figure 7, this differential gain can be exploited to determine the spectral domain associated with the outflow (i.e. the velocity interval where the low beam power spectral density exceeds that in the high beam);

(c) use of the elevation angle dependent differential phase between the low and high beams [Anderson,1988]. Given knowledge of this phase difference versus elevation angle, the weather velocity spectrum can be mapped to elevation angle subject to ambiguities caused by wrap-around of the phase pattern.

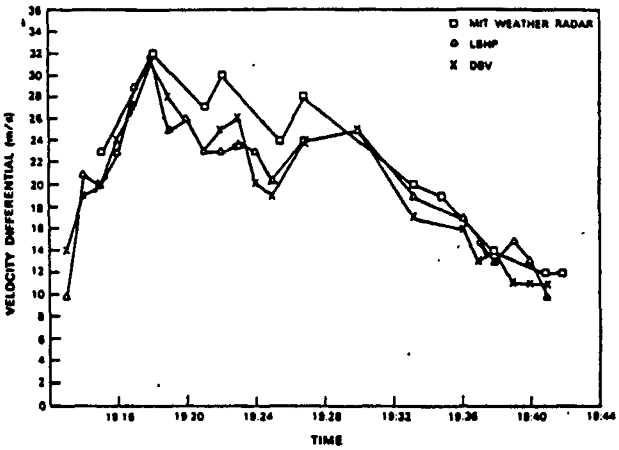

Figure 8. Pencil beam radar and ASR estimates of differential radial velocity versus time across microburst on 14 June, 1987.

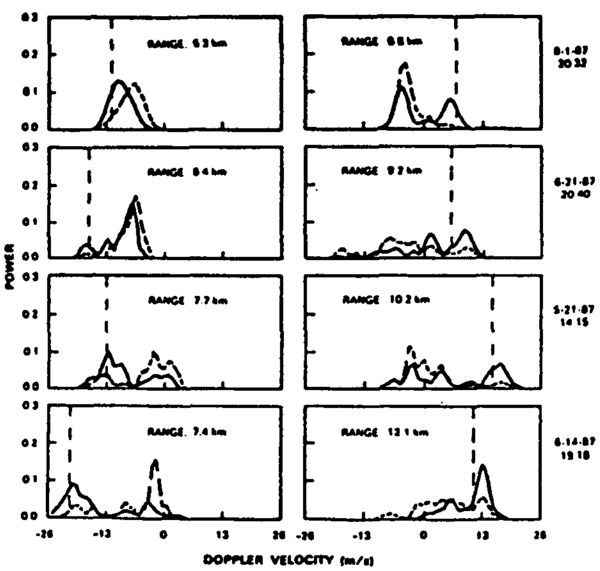

Figure 7. Velocity spectra measured in the approaching (left) and receding (right) radial velocity cores of example microbursts. Solid and dashed curves are for the low and high receiving beams respectively.

These techniques were applied offline to signals recorded from our Huntsville ASR during microbursts and the resulting velocity fields compared to those measured by the pencil beam weather radar. As an example, Figure 8 compares the temporal evolution of the radial velocity differential across a microburst as measured by the ASR and the pencil weather radar. "LBHP" and "DBV" refer to the first and second methods in the preceding paragraph. Both ASR-based estimates tracked the intensification and decay of the microburst's velocity shear; over the time period shown, the RMS difference between the ASR and weather radar velocity differential measurements was 3 m/s.

Analogous results from other wet microbursts recorded during the summers of 1987 and 1988 confirm that using suitable data processing techniques, the divergent shear signature is recognizable in the ASR-generated velocity field and that the resulting radial velocity differential measurement is in reasonable quantitative agreement with that measured by the pencil beam weather radar.

3. Automatic Microburst Detection

As an end-to-end test of ASR microburst detection capability, we applied a slightly modified version of the TDWR divergent outflow algorithm [Merritt, 1987] to radial velocity fields estimated from our ASR during microbursts in Huntsville. The algorithm's microburst declarations were "scored" against truth as determined through manual observation of the pencil beam weather radar data. The evaluation shown here included about 300 microburst signatures, all within the operationally significant range interval extending to 12 km from the radar.

Figure 9 shows the resulting performance statistics for one of the processing techniques described above--that involving comparison of low and high beam amplitude spectra. Detection and false-alarm probabilities are shown as a function of the minimum velocity shear of the microbust events or algorithm alarms that were scored. The plot indicates that 96 percent of microburst signatures with velocity shear greater than 15 m/s were automatically detected using the ASR data. Algorithm alarms reporting velocity shear greater than this value were false only 1 percent of the time.

The above, highly favorable detection and false alarm statistics confirm that a suitably modified ASR could provide reliable detection of microburst wind shear associated with heavy rain.

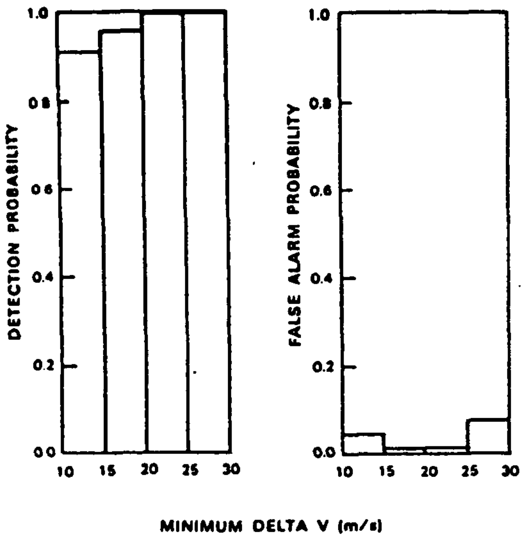

Figure 9. Probability of detection and probability of false alarm as a function of the minimum velocity shear for the microbursts that were scored.

IV. Summary

Six-level weather reflectivity reports from ASR-9's should play an important role in terminal area control. We justified in Section II our prognosis for an accurate, readily interpreted weather display -- particularly when appropriate beam shape compensations are applied. Exploratory research on the capabilities of ASRs for LAWS detection has indicated that the radars could also provide an operationally useful stand-alone capability for automatic detection of "wet" microbursts. Ongoing work will refine our understanding of this capability, quantify the potential for automatic detection of dry microbursts and gust fronts and investigate possible utilization of ASR wind measurements in conjunction with other systems such as LLWAS or TDWR.

Among current and projected sensors in the FAA's weather information network, airport surveillance radars provide a unique combination of on- or near-airport siting, rapid scan rate and large volumetric coverage. Given the near-term deployment of ASR-9's with their weather reflectivity processor and possible subsequent augmentation to include a wind shear detection capability, we expect that weather detection and display will become an increasingly important aspect of the radar's mission.

REFERENCES:

Anderson, J., *The Measurement of Doppler Wind Fields with Fast Scanning Radars: Signal Processing Techniques*, Journal of Applied Meteorology, 4, pp 627-633, 1987.

Anderson, J., *Techniques for the Detection of Microburst Outflows using Airport Surveillance Radars*, 3rd International Conference on the Aviation Weather System, Anaheim, Ca., January 30-February 3,1989.

Atlas, D., *The Detection of Low Level Windshear with Airport Surveillance Radar*, 3rd International Conference on the Aviation Weather System, Anaheim, Ca., January 30-February 3,1989.

Merritt, M., *Automatic Detection of Microburst Wind Shear for Terminal Doppler Weather Radar*, Digital Image Processing and Visual Communications Technologies in Meteorology, Cambridge, Ma., 26-28 October, 1987.

Rinehart, R., J. DiStefano and M. Wolfson, *Preliminary Memphis FAA / Lincoln Laboratory Operational Weather Studies Results*, Project Report ATC-141, Lincoln Laboratory, MIT, FAA-PM-86-40, 1987.

Smythe, G., *Evaluation of the 12 Station Enhanced Low Level Wind Shear Alert System (LLWAS) at Denver Stapleton Airport*, 3rd International Conference on the Aviation Weather System, Anaheim, Ca., January 30-February 3,1989.

Turnbull, D., J. McCarthy, J. Evans, D. Zrnic, *The FAA Terminal Doppler Weather Radar (TDWR) Program*, 3rd International Conference on the Aviation Weather System, Anaheim, Ca., January 30-February 3,1989.

Weber, M., *Assessment of ASR-9 Weather Channel Performance: Analysis and Simulation*, Project Report ATC-138, Lincoln Laboratory, MIT, FAA-PM-86-16, 1986.

Weber, M. and W. Moser, *A Preliminary Assessment of Thunderstorm Outflow Wind Measurement with Airport Surveillance Radars*, Project Report ATC-140, Lincoln Laboratory, MIT, FAA-PM-86-38, 1987.

Weber, M., *Ground Clutter Processing for Wind Measurements with Airport Surveillance Radars*, Project Report ATC-143, Lincoln Laboratory, MIT, FAA-PM-87-21, 1987.

Weber, M. and T. Noyes, *Low-Altitude Wind Shear Detection with Airport Surveillance Radars: Evaluation of 1987 Field Measurements*, Project Report ATC-159, Lincoln Laboratory, MIT, FAA-PS-88-10, 1988.